Journal of the Taiwan Institute of Chemical Engineers 89 (2018) 215–223

Contents lists available at ScienceDirect

Journal of the Taiwan Institute of Chemical Engineers

journal homepage: www.elsevier.com/locate/jtice

Reduced graphene oxide supported raspberry-like $SrWO_4$ for sensitive detection of catechol in green tea and drinking water samples

Shaktivel Manavalan[a], Mani Govindasamy[a], Shen-Ming Chen[a,*], Umamaheswari Rajaji[a], Tse-Wei Chen[a], M. Ajmal Ali[b], Fahad M.A. Al-Hemaid[b], M.S. Elshikh[b], M. Abul Farah[c]

[a] Department of Chemical Engineering and Biotechnology, National Taipei University of Technology, No.1, Section 3, Chung-Hsiao East Road, Taipei 106, Taiwan
[b] Department of Botany and Microbiology, College of Science, King Saud University, Riyadh - 11451, Saudi Arabia
[c] Department of Zoology, College of Science, King Saud University, Riyadh - 11451, Saudi Arabia

ARTICLE INFO

Article history:
Received 6 January 2018
Revised 21 April 2018
Accepted 3 May 2018
Available online 29 May 2018

Keywords:
Food analysis
Strontium tungstate
Reduced graphene oxide
Water safety
Modified electrode
Electroanalysis

ABSTRACT

The raspberry-like strontium tungstate microspheres supported on reduced graphene oxide nanosheets (rGOSs@$SrWO_4$) were prepared by a hydrothermal method and it was applied to the electrocatalytic sensing of catechol. The as-prepared rGOSs@$SrWO_4$ composite was characterized by XRD, Raman, FESEM, EDX, EIS, and voltammetric techniques. Morphology studies reveal the uniform wrapping of raspberry-like $SrWO_4$ microstructure by thin sheets of rGOSs and the composite possesses large surface area and abundant catalytic active sites. The rGOSs@$SrWO_4$ composite modified screen-printed multi-conventional electrode (SPME) was fabricated which was found to exhibit extraordinary electrocatalytic activity and excellent selectivity towards the detection of catechol. The rGOSs@$SrWO_4$/SPME displayed a linear range of 0.034–672.64 µM and detection limit of 7.34 nM using differential pulse voltammetry as signal read-out. Furthermore, the electrode was durable, reproducible and repeatable. The practical utility of the method was demonstrated in green tea and drinking water samples.

1. Introduction

Catechol (1, 2-hydroxybenzene) is a basic isomer of benzenediol, which is naturally distributed ubiquitously in plants. It has primary role in biological and industrial production activities, such as fur dyes, lubricating oils, photographic rubbers, and pharmaceuticals [1,2]. However, catechol is less degradable and toxic to the water and environmental resources [3]. As the human population increases, the need for the production of more industrial products, such as pesticides, cosmetics, medicines, tanning removers, flavoring agents, photography chemicals is increases. As a result, industrial sewages are constantly released that contaminates water resources such as, rivers, ponds, lakes, and oceans [4]. Because catechol is more attractive to the researchers to detect catechol even in low concentration and at the same time catechol to be detected in a reliable, simple and rapid manner [5,6]. Various methods are already in practice, such as capillary zone electrophoresis [7], synchronous fluorescence [8], chemiluminescence [9], high-performance liquid chromatography [10], and electrochemical methods [6,11] . Compared with traditional analytical methods, electrochemical technique is cheap, robust, rapid, high sensitive, and selective [12–14].

Recently, increasing interest has been focused on the development of catechol sensors based on metal oxide electrode modifiers [15–17]. In recent years, metal tungstate (MWO_4, M: Ca^{2+}, Sr^{2+}, Ba^{2+}, Pb^{2+} etc.) have attracted much attention due to their interesting structural and chemical properties. They have promising applications in optics and photocatalysis. On the other hand, carbonaceous materials have high conductivity, unique mechanical, excellent flexibility, good corrosion resistance and high surface area and hence they are good support materials for metal tungstates [18–20]. Yet, mostly applied materials in electrochemical applications are graphite, porous carbon, n-doped graphene, and activated carbon [21–23]. In recent years, many of transition metal oxides/hydroxides/sulfides supported on carbonaceous materials were developed for electrochemical sensing applications [24–28]. Specially, graphene supported $SrWO_4$ attracted considerable attention in many fields because $SrWO_4$ materials are low-cost, highly stable, and holding excellent electrocatalytic property for several important reactions [29].

Here, we have synthesized strontium tungstate ($SrWO_4$) microspheres enveloped reduced graphene oxide nanosheets (rGOSs) via

* Corresponding author.
E-mail addresses: smchen1957@gmail.com (S.-M. Chen), majmalaliksu@gmail.com (M. Ajmal Ali).

https://doi.org/10.1016/j.jtice.2018.05.001
1876-1070/

hydrothermal approach. The resulting composite holds excellent conductivity and very good intrinsic electrocatalytic properties. Besides, an electrochemical response for catechol at rGOSs@$SrWO_4$ shows reliable sensitivity and selectivity. The practical feasibility of the method was acquired in green tea and drinking water samples using rGOSs@$SrWO_4$ composite modified screen-printed multi-conventional electrode (SPME).

2. Experimental section

2.1. Reagents, materials and instruments

Graphite (powder, < 20 µm), $Na_2WO_4.2H_2O$, $Sr(NO_3)_3$, catechol, folic acid and all other reagents including solvents were purchased from Sigma-Aldrich and used as received. Sodium dihydrogen phosphate and disodium hydrogen phosphate were used to prepare pH. Electrochemical studies were performed in a SPME three-electrode system, which contains printed carbon as a working electrode (area 0.071 cm^2), silver as a reference electrode and printed carbon as a counter electrode. The SPME were purchased from Zensor R&D Co., Ltd., Taipei, Taiwan.

Cyclic voltammetry (CV) and differential pulse voltammetry (DPV) experiments were performed using CHI 1205A and CHI 900 electrochemical workstations (CH Instruments, Inc., U.S.A), respectively. All the electrochemical experiments are conducted at ambient conditions. Surface morphological studies were carried out using field emission scanning electron microscope (FESEM) (H-7600, Hitachi-Japan). X-ray diffraction (XRD) studies were performed in a XPERT-PRO (PANalytical B.V., The Netherlands) diffractometer using Cu Kα radiation ($k = 1.54$ Å). Raman spectra have been acquired by Micro-Raman spectrometer (RENISHAW in via system, U.K) by a 514.4 nm He/Ne laser. Energy-dispersive X-ray (EDX) spectra was recorded using Horiba Emax x-act (sensor + 24 V = 16 W, resolution at 5.9 keV = 129 eV) and EIM6ex Zahner (Kronach, Germany) was used for electrochemical impedance spectroscopy (EIS) studies.

2.2. Preparation of GOSs and synthesis of rGOSs@$SrWO_4$ composite

1 g of graphite oxide was synthesized by modified Hummer's method [30]. It was exfoliated in water through ultrasonication for 2 h to get graphene oxide nanosheets (GOSs). Then, the GOSs solution was subjected to centrifugation for 30 min at 4000 rpm to remove any unexfoliated graphite oxide. Thereafter, 5 mM of $Sr(NO_3)_2$ and 5 mM of Na_2WO_4 were added to a 25 mL of as-prepared GOSs solution and stirred for 5 min. Further, 1 mM folic acid was added, and the pH of the whole mixture was adjusted to pH 7.0 by slowly adding 0.1 M NaOH. The whole mixture was transferred into a 50 mL Teflon-lined autoclave and hydrothermally treated at 180 °C for 24 h. A white precipitate was obtained which was separated, washed (water and ethanol) and freeze-dried to yield powder of rGOSs@$SrWO_4$ composite.

2.3. Fabrication of rGOSs@$SrWO_4$ composite modified electrode

The rGOSs@$SrWO_4$ composite (1 mg mL^{-1}) was redispersed in water/ethanol (1:2; v/v) mixture through ultrasonication for 10 min. 8 µL dispersion of rGOSs@$SrWO_4$ was drop-casted at the working electrode surface of SPME using micropipette, and dried at ambient conditions. The amount of rGOSs@$SrWO_4$ covered on the work electrode surface was 8 µg and the covering area was 0.071 cm^2. Moreover, GOSs modified SPME was also prepared under same conditions for control experiments (Fig. 1).

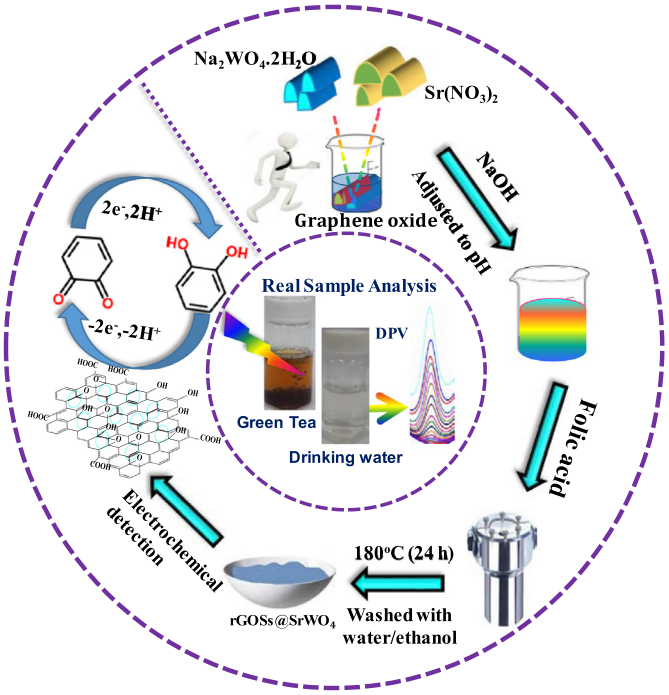

Fig. 1. Schematic representation for the hydrothermal synthesis of rGOSs@$SrWO_4$ and its electrochemical application to determining of catechol in green tea and water samples. (For interpretation of the references to color in this figure legend, the reader is referred to the web version of this article.)

3. Results and discussions

3.1. Physicochemical properties of rGOSs@$SrWO_4$

The XRD patterns of GOSs and rGOSs@$SrWO_4$ composite are shown in Fig. 2A. The XRD curve of GOSs displays a characteristic sharp peak at 2θ of 11.5° that can be correlated to the (001) planes of GOSs [31]. Interestingly, the XRD pattern of rGOSs@SrWO4 displays several additional diffraction peaks at 16.11°, 26.92°, 30.01°, 32.10°, 37.42°, 43.90°, 45.96°, 48.12°, 52.28°, 55.98°, 57.33°, 59.92°, 62.54°, 67.46°, 69.92°, 72.14°, 75.08°, 77.81°, and 79.50° that are indexed to (101), (112), (004), (200), (211), (213), (204), (220), (116), (312), (224), (215), (008), (323), (400), (208, 316), (332), (404), and (420) planes. These planes are matched with the crystal facets of $SrWO_4$ having tetragonal phase crystalline (D_4h) structure (JCPDS no.08–0490) [32]. Besides, the peak at 11.5° observed for GOSs was shifted to the expected 2θ angle of 24.85° (002), which is due to the reduction of GO to rGOSs [33].

Next, the composite was further examined by Raman spectroscopy as shown in (Fig. 2B). Both GOSs and rGOSs@$SrWO_4$ exhibit the characteristic D (related to defects in graphitic lattice) and G bands (originates from the stretching of in-plane sp^2 atoms) at 1328 and 1609 cm^{-1}, respectively [34]. The D to G band intensity ratio (I_D/I_G) was 0.933. In addition, to D and G bands, the Raman spectrum of rGOSs@$SrWO_4$ displays additional peaks, which are explained as follows. The bands at 50–150 cm^{-1} are assigned to SrO_8 polyhedra structure. The first Raman active mode B_g at 78 cm^{-1} correspond to the symmetric bending vibration of O-Sr-O, then the second active mode E_g at 99 cm^{-1} is linked to free motion of SrO_8 polyhedra structure, and the third active band E_g at 136 cm^{-1} is ascribed to symmetric stretching of O-Sr-O bond. The bands located above 150 cm^{-1} are characteristic of the WO_4 tetrahedron structure, those at 195 cm^{-1} are free rotation A_g mode. The bands A_g/B_g located at 300–400 cm^{-1} are respectively, asymmetric and symmetric bending of the E_g/B_g bands at 790–850 cm^{-1} are

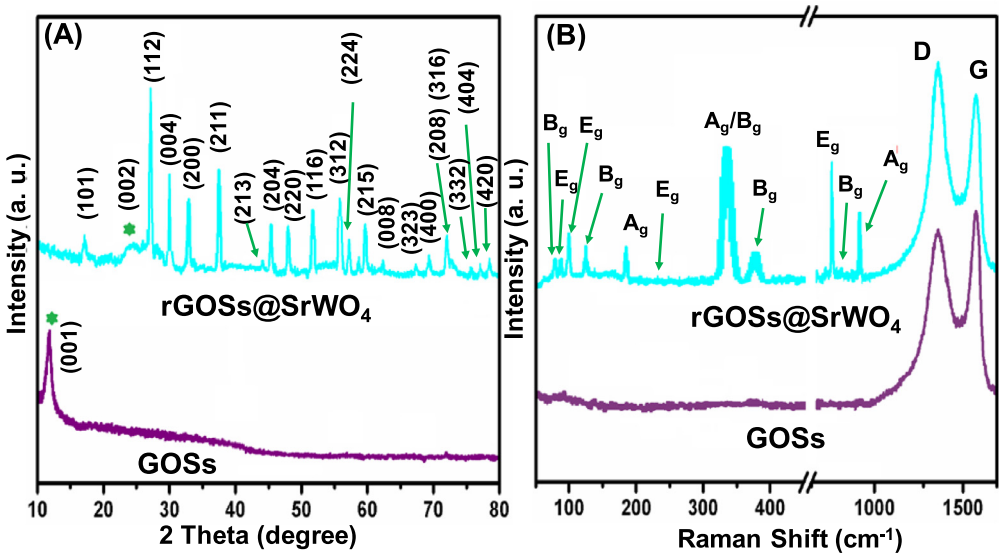

Fig. 2. (A) XRD and (B) Raman spectra of GOSs and rGOSs@$SrWO_4$ composite.

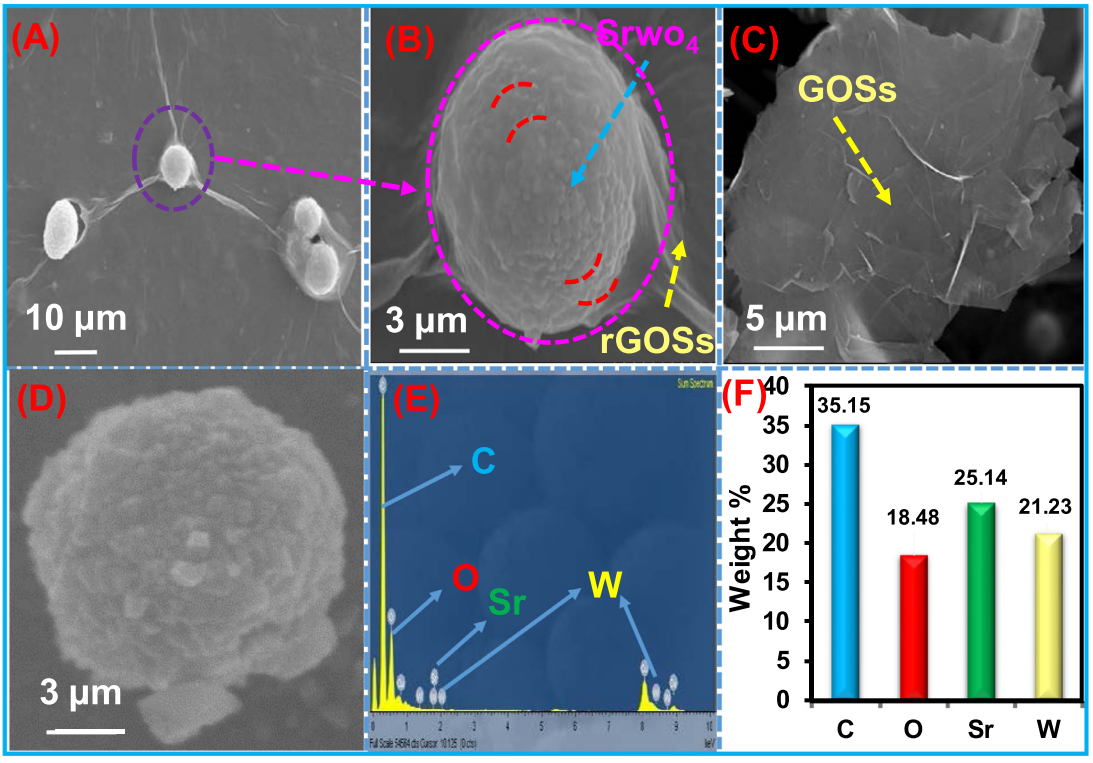

Fig. 3. FESEM images of rGOSs@$SrWO_4$ (A-B), GOSs (C), and $SrWO_4$ (D). EDX spectra (E) and corresponding quantitative analysis (F) of rGOSs@$SrWO_4$.

W-O asymmetric stretching of WO_4 tetrahedra structure. Finally, a symmetric stretching of Ag mode (–O←W→O) can be located at 934 cm^{-1}. All the characteristics Raman bands of $SrWO_4$ are consistent with previous reports [35]. In addition, the value of I_D/I_G was increased to 1.14, suggesting the increased defect density in the composit.

The FESEM image of rGOSs@$SrWO_4$ composite, (A, B), GOSs (C), and $SrWO_4$ (D) are depicted in Fig. 3. The SEM image of GO shows typical wrinkled sheet-like morphology. Microsphere-like porous morphology was observed for the $SrWO_4$. The rGOSs@$SrWO_4$ displays raspberry-like $SrWO_4$ microsphere wrapped and covered by layered GOSs (Fig. 3A, B). Thus, the hydrothermal-assisted self-assembly of $SrWO_4$ on GOSs substrate leads to the formation of GOSs supported $SrWO_4$ nanocomposite. The average particle size of $SrWO_4$ microsphere was 8 to 10 µm. The EDX spectra (Fig. 3E) of rGOSs@$SrWO_4$ shows the expected elements C, O, Sr and W. The quantitative elemental analysis provides weight percentages of 35.15%, 18.45%, 25.14%, and 21.23% for C, O, Sr and W respectively.

3.2. Electrochemical behavior of rGOSs@$SrWO_4$

EIS analysis was performed to understand the electrode-electrolyte interfacial properties. The impedance spectra were represented as Nyquist plots. The semicircle part at higher frequencies

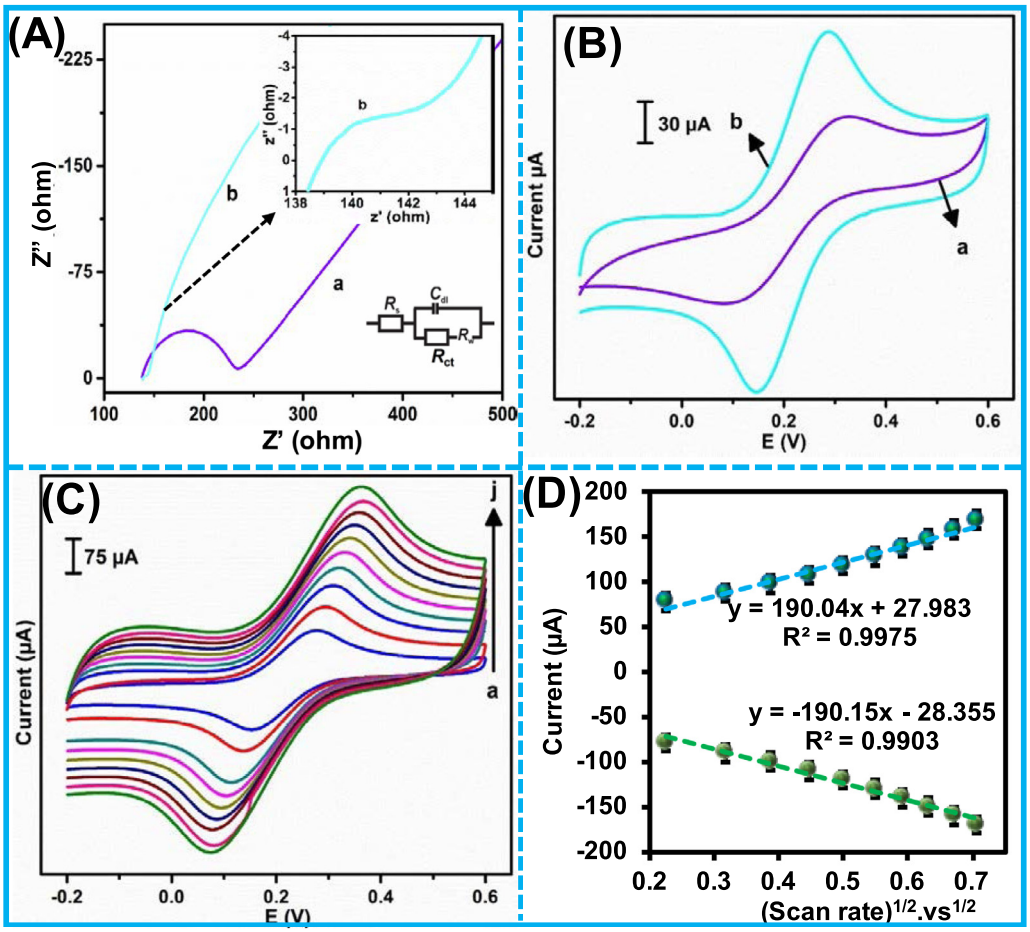

Fig. 4. (A) EIS spectra of GOSs/SPME (a), and rGOSs@$SrWO_4$/SPME (b) Inset: Randles equivalent circuit model, R_s = electrolyte resistance, R_{ct} = charge transfer resistance C_{dl} = double layer capacitance and Z_w = Warburg impedance. (B) CVs of GOSs/SPME, and rGOSs@$SrWO_4$/SPME in 0.1 M KCl + 5 mM $[Fe(CN)_6]^{3-/4-}$ at scan rate of 50 mVs^{-1}. (C) CVs of rGOSs@$SrWO_4$/SPME in 0.1 M KCl + 5 mM $[Fe(CN)_6]^{3-/4-}$ at different scan rates (a to j; 0.02–0.2 Vs^{-1}) and corresponding linear calibration plot (D).

is related to electron transfer limited process and the linear part at lower frequency region is related to diffusion-limited process. Fig. 4A shows the EIS curves obtained at GOSs (a) and rGOSs@$SrWO_4$ (b) modified electrodes in 0.1 M KCl containing 5 mM $Fe(CN)_6^{3-/4-}$. The frequency range was 0.1 Hz–1 MHz and the amplitude was 5 mV. Randles equivalent circuit model was used to fit the experimental data (inset to Fig. 4A). The parameters are electrolyte resistance (R_s), charge transfer resistance (R_{ct}), double layer capacitance (C_{dl}) and Warburg impedance (Z_w), respectively. The R_{ct} values obtained at GO (curve a) and rGOSs@$SrWO_4$ (curve b) film modified electrodes are 105 Ω, and 16 Ω. The EIS result indicates resistance at rGOSs@$SrWO_4$ has been considerably reduced, which is ascribed to the excellent electronic conductivity property of rGOSs@$SrWO_4$ composite.

The electrochemical behavior of GOSs/SPME and rGOSs@$SrWO_4$/SPME was probed by cyclic voltammetry. 0.1 M KCl was used as supporting electrolyte and 5 mM $[Fe(CN)_6]^{3-/4-}$ was used as redox probe. The CV curves of GOSs/SPME and rGOSs@$SrWO_4$/SPME shows a pair of well-defined redox peaks related to the redox reaction of $[Fe(CN)_6]^{3-/4-}$ (Fig. 4B). The peak-to-peak potential separation (ΔE_p) values are 248, and 134 mV at GOSs/SPME and rGOSs@$SrWO_4$/SPME respectively. Compared to GOSs/SPME, the rGOSs@$SrWO_4$/SPME shows higher redox peak currents and smaller peak-to-peak potential separation. The insulating nature of GOSs blocks the diffusion of $[Fe(CN)6]^{3-/4-}$ and increased the internal resistance at the electrode interface (curve a). On the other hand, the higher electronic conductivity property of rGOSs@$SrWO_4$/SPME facilitates highly enhanced redox peak currents and the observed low ΔE_p indicates the composite considerably promotes the electron transfer reactions.

Fig. 4C shows the CVs of rGOSs@$SrWO_4$/SPME towards $[Fe(CN)_6]^{3-/4-}$ at varied scan rates from 0.03–0.3 V s^{-1} and corresponding plot between peak current and square root of scan rate is given in Fig. 4D. The electrochemical active surface area of the modified SPME was assessed by substituting slope value of different scan rate plot in Randles–Sevcik Eq. (1) [36].

$$i_p = 2.72 * 10^5 n^{3/2} A D^{1/2} C \upsilon^{1/2} \quad (1)$$

Here, i_p is peak current, n is number of electrons involved in the redox reaction, transfer, υ is scan rate (Vs^{-1}), A is electrochemical active area (cm^2), D is the diffusion coefficient (cm^2 s^{-1}), C is the concentration of $[Fe(CN)_6]^{3-/4-}$ (mol cm^{-3}). The electrochemically active surface areas were calculated to be 0.021, and 0.086 cm^2 for GOSs/SPME and rGOSs@$SrWO_4$/SPME respectively. Thus, the active area of rGOSs@$SrWO_4$/SPME is 4.1 fold higher than the area of GOSs/SPME, indicating that the rGOSs@$SrWO_4$/SPME is suitable for electrocatalytic sensing applications.

3.3. Electrocatalysis of catechol at rGOSs@$SrWO_4$

Next, the electrocatalytic performance of rGOSs@$SrWO_4$ towards catechol was studied by CV. Fig. 5A displays the CVs of unmodified, $SrWO_4$, GOSs, and rGOSs@$SrWO_4$ modified SPMEs in phosphate buffer (pH 7.0) and scan rate of 0.05 V s^{-1} was applied. As shown in figure, the rGOSs@$SrWO_4$/SPME exhibited a well-defined redox peaks ascribed to the redox reaction of

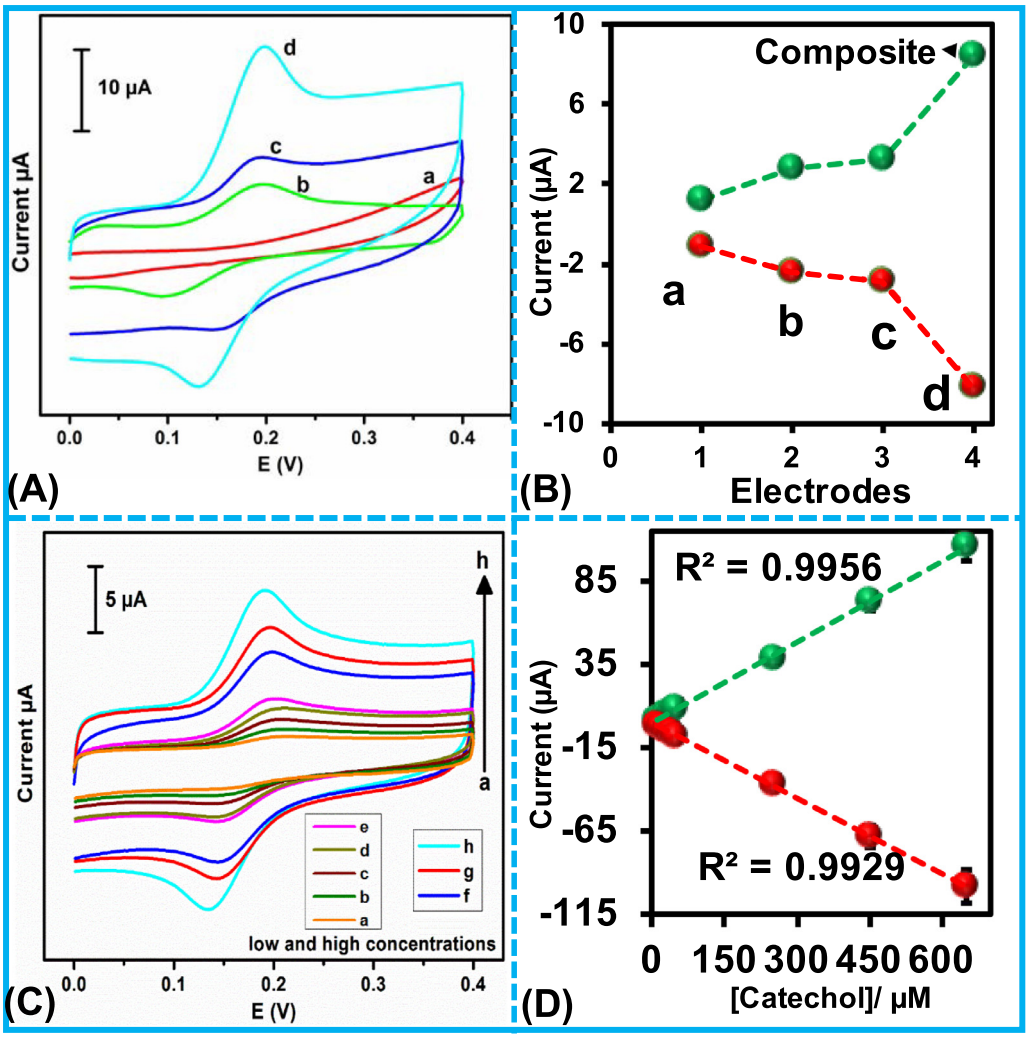

Fig. 5. (A) CVs obtained at unmodified SPME (a), $SrWO_4$/SPME (b), GOSs/SPME (c), and rGOSs@$SrWO_4$/SPME (d) in phosphate buffer (pH 7.0) containing 5 μM catechol at the scan rate of 0.05 V s^{-1}. (B) Different electrodes vs. corresponding peak currents. (C) CVs of the rGOSs@$SrWO_4$/SPME in 0.1 M PB solution (pH 7) with various concentrations of catechol (a to h; 10–650 μM) at 0.05 Vs^{-1} scan rate. (D) peak current vs. concentration of catechol.

catechol. In this reaction 1,2-dihydroxybenzene (catechol) is convert to benzoquinone. GOSs/SPME displays feeble redox peaks, while unmodified SPME does not shows any obvious redox peaks. For instance, rGOSs@$SrWO_4$ displays 2.69, 2.92 and 6.76 fold larger redox peak currents than GOSs/SPME, $SrWO_4$/SPME and unmodified SPME, respectively (Fig. 5B). Clearly, rGOSs@$SrWO_4$ nanocomposite modification on SPME surface enables amplified current signal as well as accelerated electron transfer. The synergic effect between rGOSs and $SrWO_4$ could have significant contribution to the observed improved electrocatalysis; this effect is well established for graphene-based nanocomposites.

Fig. 5C presented the CVs obtained at rGOSs@$SrWO_4$/SPME in 0.1 M phosphate buffer (pH 7.0) containing varied concentrations of catechol. As shown in figure, the oxidation (I_{pa}) and reduction peak currents (I_{pc}) were increased linearly, as the concentration of catechol increases. The plot between peak currents and concentration of catechol exhibits good linearity (Fig. 5D). The corresponding regression equations are, Fig. 5D, I_{pa} (μA) = 0.1615 (μM) + 0.166 (R^2 = 0.996) and I_{pc} (μA) = 0.1509 (μM) – 0.166 (R^2 = 0.993).

3.4. Kinetic studies

Fig. 6A shows the CVs of rGOSs@$SrWO_4$/SPME towards 5 μM catechol at different scan rates. Both faradaic and non-faradaic currents are increased as the scan rate increases from 0.02 to 0.22 V s^{-1}. The oxidation peak shifted towards positive potential, while the reduction peak shifted towards negative potential. Besides, the redox peak current and square root of the scan rate exhibited good linearity, a characteristic behavior of a diffusion controlled electrocatalytic process (Fig. 6B). The linear regression equations for the corresponding scan rate plot are I_{pa} (μA) = 3.356$\nu^{1/2}$ (Vs^{-1})$^{1/2}$ + 130.06; R^2 = 0.993 and I_{pc} (μA) = –9.330$\nu^{1/2}$ (Vs^{-1})$^{1/2}$ + 129.45; R^2 = 0.995. Also, the oxidation peak potential (E_p) shifts to higher positive potentials with the increase in scan rate (Fig. 6C). A plot of E_p vs square root of the scan rate displays a linear relationship which implies that catechol electrocatalytic oxidation process is chemically reversible (Fig. 6C).

3.5. Determination of catechol by DPV

Fig. 7A presents the DPV curves obtained at rGOSs@$SrWO_4$/SPME towards varied concentrations of catechol in phosphate buffer (pH 7.0) as supporting electrolyte. The optimized parameters used to record DPV are, pulse amplitude = 0.05 V, pulse width = 0.05 s, pulse period = 0.2 s, sampling width = 0.0167 s and quite time = 4 s. Sharp electrocatalytic response was observed for each concentrations of catechol. The I_{pa} increases linearly as the

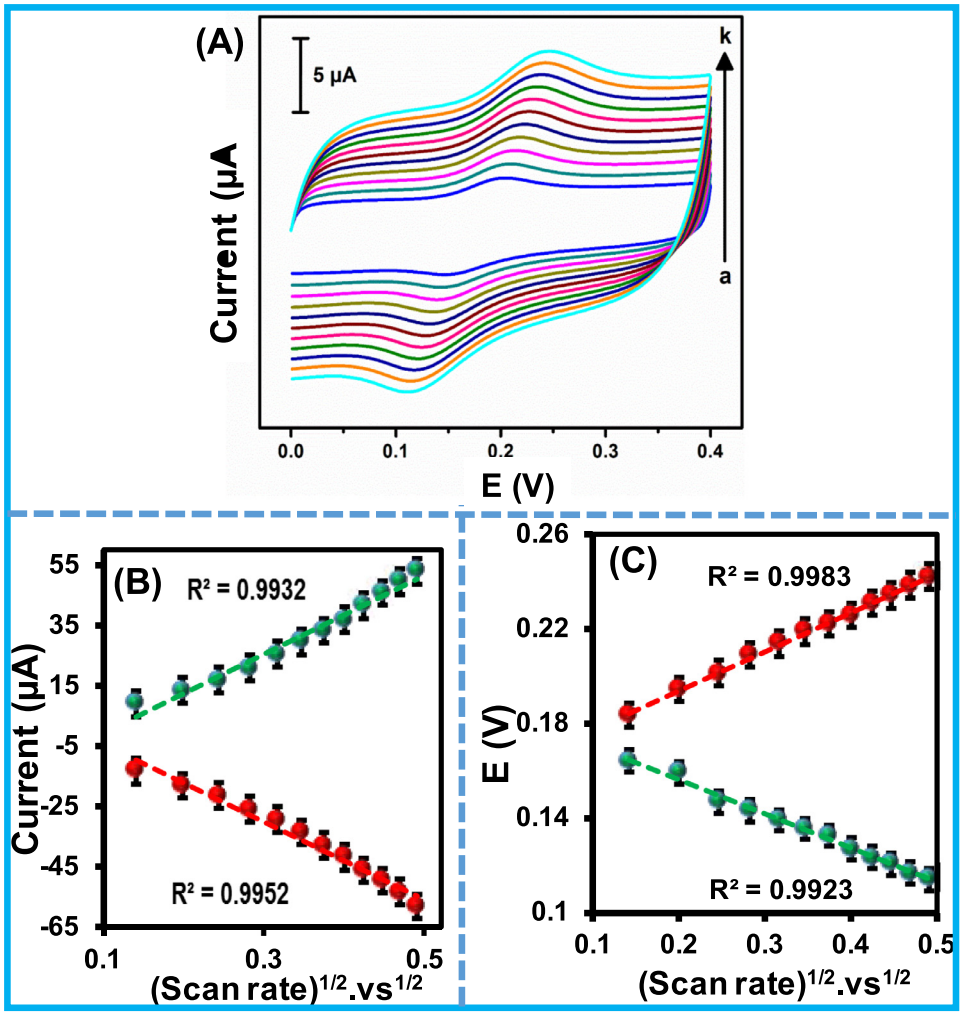

Fig. 6. Shows CVs obtained at rGOSs@$SrWO_4$/SPME in phosphate buffer (pH 7.0) containing 5 µM catechol at different scan rates (a to k; 0.02 to 0.22 V s^{-1}). (B) plot of I_{pa} and I_{pc} versus square root of scan rates. (C) Plot of E_p versus square root of scan rates.

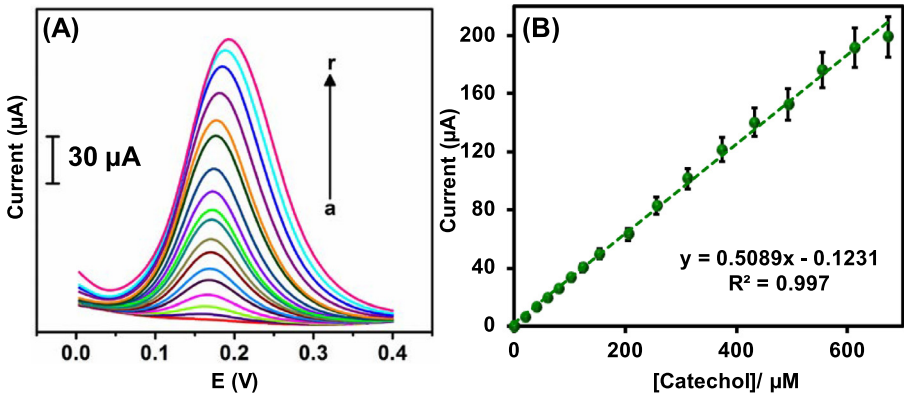

Fig. 7. (A) DPVs of rGOSs@$SrWO_4$/SPME towards varied concentrations of catechol (a–q; 0.034–672.64 µM) in phosphate buffer (pH 7.0) and corresponding linear regression plot between peak currents (µA) and concentrations of catechol.

concentrations of catechol increases. A linear calibration between plot between concentration of catechol and corresponding peak current displays good linearity (Fig. 7B). The regression equation was obtained as, [I] (µA) = 0.5089 [catechol] (µA/µM) + 1.78; R^2 = 0.997. The linear range was 0.034–672.64 µM. The sensitivity was 7.167 µAµM^{-1} cm^{-2}. The detection limit was calculated to be 7.34 nM. The limit of detection (LOD) was calculated using the formula, LOD = 3 s_b/S (where, s_b = standard deviation of blank signal and S = sensitivity). The limit of quantification (LOQ) of the method was 24.5 nM. The linear range, detection limit and sensitivity of the electrodes were compared with previous reports (Table 1). From the table, we infer that rGOSs@$SrWO_4$/SPME film modified electrode delivered either comparable or better analytical performance over existing modified electrodes. Remarkably, the

Table 1
Comparison of catechol sensing performance at rGOSs@$SrWO_4$/SPME with previous literature.

Electrodes	Linear range (μM)	LOD (nM)	Reference
CNS[a]-CNT[b]	1–200	90.0	[37]
COOH-CNT/CT[c]/Au	5–900	89.0	[15]
N-CNT@CNF[d]	0.08–350	20.0	[38]
Polyimide/RGO[e]-Au	2–1289	20.0	[39]
Pd/Cu-CNTs	1–280	60.0	[40]
Au/EGPE[f]	0.5–100	27.0	[16]
MOF-ERGO[g]	0.1–566	100.0	[41]
Graphene oxide	1–350	182.0	[42]
Meso-Co_3O_4	1–500	100.0	[43]
Chitin/graphite	0.3–110.6	85.0	[44]
N, S-graphene	10–70	150.0	[17]
NiO/MWCNT	7.4–56	150.0	[45]
rGOSs@$SrWO_4$	0.034–672.64	7.34	This work

[a] carbon nitride nanosheets, [b]carbon nanotube, [c]chitosan, [d]carbon nanofibers, [e]reduced graphene oxide, [f]exfoliated graphite paper electrode, [g]electrochemically reduced graphene oxide.

detection limit was 7.34 nM, which reveals that the rGOSs@$SrWO_4$ greatly contributed to the signal amplification.

3.6. Selectivity and stability of the sensor

The selectivity of the catechol sensor is more important especially in the presence of high concentration of hydroquinone (HQ), since it could easily interfere with the oxidation signal of catechol due to the similar structural features (isomer) and chemical activity. The selectivity of rGOSs@$SrWO_4$-modified electrode towards varied concentrations of catechol in presence of fixed concentration of HQ (0.2 mM) had been analyzed and the results are presented in Fig. S1A. It can be seen that the oxidation peaks of HQ and catechol are displayed at two different potentials with wide potential gap. Evidently, the voltammetric response of HQ was not interfered the response of catechol. A linear dependence of the observed oxidation peak current (I_{pa}) with varied concentration of catechol (5 – 35 μM) was observed even in presence of high concentrations of HQ.

In addition, biological molecules, and metal ions based interfering compounds are tested for their possible interferences with our catechol sensing system. The electrocatalytic response of modified electrode towards 25 μM of catechol and each 0.2 mM of quercetin (QT), dopamine (DA), ascorbic acid (AA), uric acid (UA), acetaminophen (AAP), glucose (Glu), epinephrine (EP), norepinephrine (NEP), Cu^{2+}, Na^{+}, I^{-}, Ni^{2+}, Zn^{2+}, Cl^{-}, Cd^{2+}, Hg^{2+}, and Cr^{2+}were also examined (Fig. S2A). As shown in figure, none of these compounds shown detectable signals. Possibly, the π stacking interaction between rGOSs and phenyl moiety of catechol provides selectivity. This π interaction avoids interference from compounds, which are do not having phenyl moieties. Besides, the presence of edge-functionalized rGOSs makes the electrode attractive for para and ortho directed pieces in benzodiol isomeric mixtures (catechol and hydroquinone). Nevertheless, our results indicated the voltammetric signal of hydroquinone is different from the signal of catechol, thus allowing us to discriminate their signals. Thus, the selectivity study indicates rGOSs@$SrWO_4$/SPME holds excellent selectivity in presence of possible biological compounds as well as metal ions.

3.7. Stability, repeatability and reproducibility

In order to determine storage stability of rGOSs@$SrWO_4$ composite modified SPME, its electrocatalytic response towards 5 μM catechol was monitored every day. The modified SPME was kept stored in phosphate buffer (pH 7.0) at 4 °C when not in use. During 10 days storage period, the modified electrode presented well defined catalytic response. About 96.87% of the initial response current was retained over 10 days of its continuous use revealing good storage stability (Fig. S2B). Next, repeatability and reproducibility of the modified electrode have been tested towards 5 μM catechol in phosphate buffer (pH 7.0). The modified SPME exhibited appreciable repeatability with relative standard deviation of 3.24% for 5 repetitive measurements carried out using single SPME. In addition, it exhibits promising reproducibility of 3.74% for the five independent measurements carried out in five different composite modified SPMEs.

3.8. Real sample analysis

The practical utility of rGOSs@$SrWO_4$ composite modified electrode was demonstrated in drinking water and green tea samples (Figs. 8 and 9). The drinking water and green tea samples are found to be catechol free through DPV analysis. Then, a known amount of catechol was spiked prior to analysis. The spiked catechol concentrations were added different additions. Next, the amount of catechol spiked in the samples (drinking water + catechol and green tea + catechol) was tested using the rGOSs@$SrWO_4$ composite modified electrode. The sensor was delivered sharp peaks as lab sample (Figs. 8A and 9A). The linear ranges (drinking water + catechol = 0.035–270 μM and green

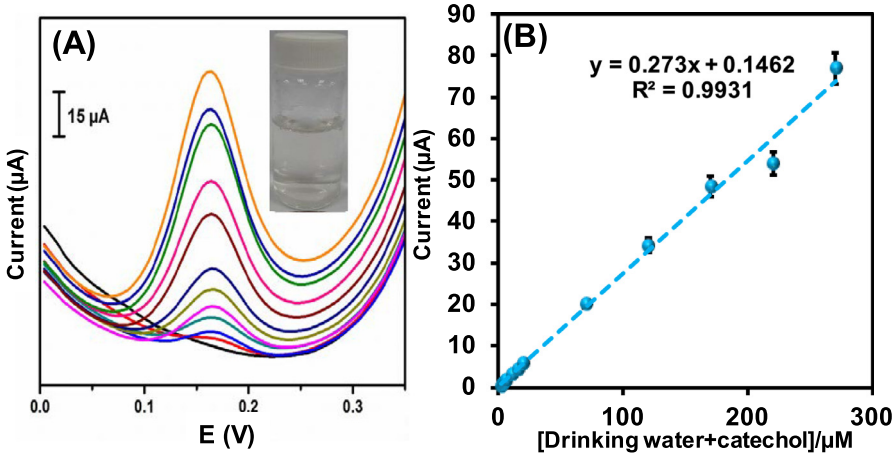

Fig. 8. (A) DPVs of rGOSs@$SrWO_4$ composite modified SPME containing various concentrations of catechol containing drinking water samples in PB solution (pH 7.0) at a scan rate of 0.05 V s^{-1}, (B) Corresponding calibration plot for peak currents vs. [catechol]/μM.

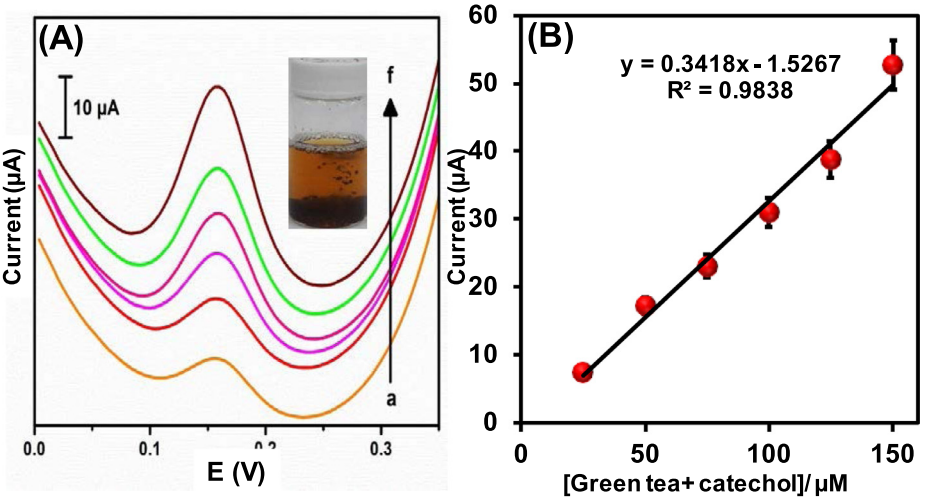

Fig. 9. (A) DPVs of rGOSs@$SrWO_4$ composite modified SPME containing various concentrations of catechol containing green tea samples in phosphate buffer (pH 7.0) at a scan rate of 0.05 V s^{-1}, (B) Corresponding calibration plot for peak currents vs. concentrations of catechol (25 –150 µM). (For interpretation of the references to color in this figure legend, the reader is referred to the web version of this article.)

Table 2
Determination of catechol (CT) in drinking water and green tea samples using rGOSs@$SrWO_4$ composite modified electrode by DPV and HPLC method.

Sample	Spiked (µM)	Found[#] (µM)	Accuracy (%)	Found* (µM)	Accuracy (%)
CT	0.0	0.0	–	0.0	–
CT + drinking	10.0	9.94	99.4	9.43	94.3
water	20.0	19.84	99.2	19.34	96.7
CT + green	10.0	9.94	99.4	9.27	92.7
tea	20.0	19.83	99.15	19.11	95.5

[#] Detected by Waters Alliance, model 2695 HPLC (Empower, version 3). *Detected by rGOSs@$SrWO_4$ composite modified electrode by DPV ($n = 3$).

tea + catechol = 25–150 µM), and limit of detection values are presented in Table S1. Hence, the rGOSs@$SrWO_4$ composite modified electrode has good practical feasibility. We established a sensitive electrochemical detection method for the quantification of catechol in water and green tea samples.

The practical ability of the sensor was compared to traditional HPLC method and DPV. The catechol sensor was evaluated in catechol spiked drinking water and green tea samples from the laboratory using DPV method. The recovery values were calculated using the standard addition method. In addition, the catechol was also detected by traditional HPLC analysis. The detected values of catechol by HPLC and electrochemical methods were tabulated in Table 2. It can be seen that the results are showed good accuracy to the results obtained by HPLC method for detection of catechol (Table 2). The result clearly validates that the proposed rGOSs@$SrWO_4$ composite modified electrode can be used for real-time sensing of catechol.

4. Conclusions

In this work, a novel and eco-friendly electrocatalyst of reduced graphene oxide covered strontium tungstate composite was synthesized. The composite was characterized by FESEM, EDX, XRD, Raman, and EIS. The composite was provided a large electroactive surface area and high electrocatalytic activity. The rGOSs@$SrWO_4$ composite modified electrode shown excellent electrochemical detection performance of catechol. DPV sensing platform was demonstrated which showed wide linear range (0.034–672.64 µM) and nanomolar detection limit (7.34 nM). The method was successful in the determination of catechol spiked in drinking water and green tea samples, thus as great potential in food safety and water analysis. In future rGOSs@$SrWO_4$ composite will be studied on photodegradation and photo-water splitting applications.

Acknowledgment

The authors extend their appreciation to the Deanship of Scientific Research at King Saud University for funding this work through research group no (RG-195). This work was supported by the Ministry of Science and Technology, Taiwan (MOST 106-2113-M-027-003).

Supplementary materials

Supplementary material associated with this article can be found, in the online version, at doi:10.1016/j.jtice.2018.05.001.

References

[1] Liu L, Ma Z, Zhu X, Alshahrani L-A, Tie S, Nan J. A glassy carbon electrode modified with carbon nano-fragments and bismuth oxide for electrochemical analysis of trace catechol in the presence of high concentrations of hydroquinone. Microchim Acta 2016;183:3293–301.
[2] Li J, Xia J, Zhang F, Wang Z, Liu Q. An electrochemical sensor based on copper-based metal-organic frameworks-graphene composites for determination of dihydroxybenzene isomers in water. Talanta 2018;181:80–6.
[3] De Luis A, Lombraña J, Menendez A, Sanz J. Analysis of the toxicity of phenol solutions treated with H_2O_2/UV and H_2O_2/Fe oxidative systems. Ind Eng Chem Res 2010;50:1928–37.
[4] Arago M, Arino C, Dago A, Diaz-Cruz J-M, Esteban M. Simultaneous determination of hydroquinone, catechol and resorcinol by voltammetry using graphene screen-printed electrodes and partial least squares calibration. Talanta 2016;160:138–43.
[5] Liu X, Jiang H, Lei J, Ju H. Anodic electrochemiluminescence of CdTe quantum dots and its energy transfer for detection of catechol derivatives. Anal Chem 2007;79:8055–60.
[6] Lakshmi D, Bossi A, Whitcombe M-J, Chianella I, Fowler S-A, Subrahmanyam S, Piletska E-V, Piletsky S-A. Electrochemical sensor for catechol and dopamine based on a catalytic molecularly imprinted polymer-conducting polymer hybrid recognition element. Anal Chem 2009;81:3576–84.
[7] Wallingford R-A, Ewing A-G. Separation of serotonin from catechols by capillary zone electrophoresis with electrochemical detection. Anal Chem 1989;61:98–100.

[8] Luster J, Lloyd T, Sposito G, Fry I-V. Multi-wavelength molecular fluorescence spectrometry for quantitative characterization of copper (II) and aluminum (III) complexation by dissolved organic matter. Environ Sci Technol 1996;30:1565–74.

[9] Peng Y, Dong Y, Ai M, Ding H. Electrogenerated chemiluminescence of Ag_2Te quantum dots and its application in sensitive detection of catechol. J Lumin 2017;190:221–7.

[10] Carmella SG, Hecht SS, Tso T, Hoffmann D. Roles of tobacco cellulose, sugars, and chlorogenic acid as precursors to catechol in cigarette smoke. J Agric Food Chem 1984;32:267–73.

[11] Senthil Kumar A, Swetha P. Electrochemical-assisted encapsulation of catechol on a multiwalled carbon nanotube modified electrode. Langmuir 2010;26:6874–7.

[12] Govindasamy M, Mani V, Chen S-M, Chen T-W. Sundramoorthy A-K. Methyl parathion detection in vegetables and fruits using silver@graphene nanoribbons nanocomposite modified screen printed electrode. Sci Rep 2017;7:46471.

[13] Guo S, Wen D, Zhai Y, Dong S, Wang E. Platinum nanoparticle ensemble-on–graphene hybrid nanosheet: one-pot, rapid synthesis, and used as new electrode material for electrochemical sensing. ACS nano 2010;4:3959–68.

[14] Muthumariappan A, Govindasamy M, Chen S-M, Sakthivel K, Mani V. Screen-printed electrode modified with a composite prepared from graphene oxide nanosheets and Mn_3O_4 microcubes for ultrasensitive determination of nitrite. Microchim Acta 2017;184:3625–34.

[15] Shen Y, Rao D, Sheng Q, Zheng J. Simultaneous voltammetric determination of hydroquinone and catechol by using a glassy carbon electrode modified with carboxy-functionalized carbon nanotubes in a chitosan matrix and decorated with gold nanoparticles. Microchim Acta 2017;184:3591–601.

[16] Fan L, Li X, Kan X. Disposable graphite paper based sensor for sensitive simultaneous determination of hydroquinone and catechol. Electrochim Acta 2016;213:504–11.

[17] Xiao L, Yin J, Li Y, Yuan Q, Shen H, Hu G, Gan W. Facile one-pot synthesis and application of nitrogen and sulfur-doped activated graphene in simultaneous electrochemical determination of hydroquinone and catechol. Analyst 2016;141:5555–62.

[18] Sheng Z-H, Shao L, Chen J-J, Bao W-J, Wang F-B, Xia X-H. Catalyst-free synthesis of nitrogen-doped graphene via thermal annealing graphite oxide with melamine and its excellent electrocatalysis. ACS nano 2011;5:4350–8.

[19] Chen S-M, Umamaheswari R, Mani G, Chen T-W, Ali M-A, Fahad A-H, Elshikh M, Farah M-A. Hierarchically structured $CuFe_2O_4$ ND@RGO composite for the detection of oxidative stress biomarker in biological fluids. Inorg Chem Front 2018;5:944.

[20] Mani V, Chen T-W, Selvaraj S. MWCNTs/MoS_2 Decorated Cobalt Oxide Polyhedrons Composite Film Modified Electrode for Electrochemical Determination of Dopamine in Rat Brain and Human Blood Serum Samples. Int J Electrochem Sci 2017;12:7435–45.

[21] Wang Y, Shao Y, Matson D-W, Li J, Lin Y. Nitrogen-doped graphene and its application in electrochemical biosensing. ACS Nano 2010;4:1790–8.

[22] Wei P, Shen J, Wu K, Hu C. Tuning electrochemical behaviors of N-methyl-2-pyrrolidone liquid exfoliated graphene nanosheets by centrifugal speed-based grading. Carbon 2018;129:183–90.

[23] Govindasamy M, Chen S-M, Mani V, Akilarasan M, Kogularasu S, Subramani B. Nanocomposites composed of layered molybdenum disulfide and graphene for highly sensitive amperometric determination of methyl parathion. Microchim Acta 2017;184:725–33.

[24] Hu L, Cheng Q, Chen D, Ma M, Wu K. Liquid-phase exfoliated graphene as highly-sensitive sensor for simultaneous determination of endocrine disruptors: Diethylstilbestrol and estradiol. J Hazard Mater 2015;283:157–63.

[25] Hao J, Ji L, Wu K, Yang N. Electrochemistry of ZnO@ reduced graphene oxides. Carbon 2018;130:480–6.

[26] Soomro R-A, Hallam K-R, Ibupoto Z-H, Tahira A, Sherazi S-T-H, Juddin S, Jawaid S, Willander M. Glutaric acid assisted fabrication of CuO nanostructures and their application in development of highly sensitive electrochemical sensor system for carbamates. Electroanalysis 2016;28:1634–40.

[27] Soomro R-A, Hallam K-R, Ibupoto Z-H, Tahira A, Sherazi S-T-H, Memon S-S, Willander M. Amino acid assisted growth of CuO nanostructures and their potential application in electrochemical sensing of organophosphate pesticide. Electrochim Acta 2016;190:972–9.

[28] Govindasamy M, Chen S-M, Mani V, Devasenathipathy R, Umamaheswari R, Santhanaraj K-J, Sathiyan A. Molybdenum disulfide nanosheets coated multiwalled carbon nanotubes composite for highly sensitive determination of chloramphenicol in food samples milk, honey and powdered milk. J Colloid Interf Sci 2017;485:129–36.

[29] Dirany N, McRae E, Arab M. Morphological and structural investigation of $SrWO_4$ microcrystals in relationship with the electrical impedance properties. Cryst Eng Com 2017;19:5008–21.

[30] Hummers W-S Jr, Offeman R-E. Preparation of graphitic oxide. J Am Chem Soc 1958;80:1339.

[31] Kosynkin D-V, Higginbotham A-L, Sinitskii A, Lomeda J-R, Dimiev A, Price B-K, Tour JM. Longitudinal unzipping of carbon nanotubes to form graphene nanoribbons. Nature 2009;458:872–6.

[32] Zhang L, Wang W, Zhou L, Xu H. Bi_2WO_6 nano-and microstructures: shape control and associated visible-light-driven photocatalytic activities. Small 2007;3:1618–25.

[33] Ujjain S-K, Singh G, Sharma RK. Co_3O_4@reduced graphene oxide nanoribbon for high performance asymmetric supercapacitor. Electrochim Acta 2015;169:276–82.

[34] Ramachandran R, Saranya M, Kollu P, Raghupathy B-P, Jeong S-K. Grace A-N. Solvothermal synthesis of Zinc sulfide decorated Graphene (ZnS/G) nanocomposites for novel Supercapacitor electrodes. Electrochim Acta 2015;178:647–57.

[35] Sun L, Guo Q, Wu X, Luo S, Pan W, Huang K, Lu J, Ren L, Cao M, Hu C. Synthesis and photoluminescent properties of strontium tungstate nanostructures. J Phys Chem C 2007;111:532–7.

[36] Daum P, Lenhard J, Rolison D, Murray R-W. Diffusional charge transport through ultrathin films of radiofrequency plasma polymerized vinylferrocene at low temperature. J Am Chem Soc 1980;102:4649–53.

[37] Zhang H, Huang Y, Hu S, Huang Q, Wei C, Zhang W, Yang W, Dong P, Hao A. Self-assembly of graphitic carbon nitride nanosheets–carbon nanotube composite for electrochemical simultaneous determination of catechol and hydroquinone. Electrochim Acta 2015;176:28–35.

[38] Guo Q, Zhang M, Zhou G, Zhu L, Feng Y, Wang H, Zhong B, Hou H. Highly sensitive simultaneous electrochemical detection of hydroquinone and catechol with three-dimensional N-doping carbon nanotube film electrode. J Electroanal Chem 2016;760:15–23.

[39] Shen X, Xia X, Du Y, Wang C. Electroless deposition of Au nanoparticles on reduced graphene oxide/polyimide film for electrochemical detection of hydroquinone and catechol. Front Mater Sci 2017;11:262–70.

[40] Sabbaghi N, Noroozifar M, Tohidinia M, Farsadrooh M. Modified Glassy Carbon Electrode with Galvanized Copper Nanowires by Palladium and Carbon Nanotubes for Speciation of Dihydroxybenzene Isomers. Int J Electrochem Sci 2017;12:8777–92.

[41] Chen Q, Li X, Min X, Cheng D, Zhou J, Li Y, Xie Z, Liu P, Cai W, Zhang C. Determination of catechol and hydroquinone with high sensitivity using MOF–graphene composites modified electrode. J Electroanal Chem 2017;789:114–22.

[42] Velmurugan M, Karikalan N, Chen S-M, Cheng Y-H, Karuppiah. Electrochemical preparation of activated graphene oxide for the simultaneous determination of hydroquinone and catechol. J Colloid Interf Sci 2017;500:54–62.

[43] Cui S, Li L, Ding Y, Zhang J. Mesoporous cobalto-cobaltic oxide modified glassy carbon electrode for simultaneous detection of hydroquinone and catechol. J Electroanal Chem 2016;782:225–32.

[44] Palanisamy S, Thangavelu K, Chen S-M, Velusamy V, Chen T-W, Kannan R-S. Preparation and characterization of a novel hybrid hydrogel composite of chitin stabilized graphite: Application for selective and simultaneous electrochemical detection of dihydroxybenzene isomers in water. J Electroanal Chem 2017;785:40–7.

[45] Goulart L-A, Mascaro L-H. GC electrode modified with carbon nanotubes and NiO for the simultaneous determination of bisphenol A, hydroquinone and catechol. Electrochim Acta 2016;196:48–55.